DOI 10.5162/16dss2022/P31

Electronics for Continuously Measuring the Resonance Frequency and Attenuation of a Split-Ring Resonator

Martin Lippmann, Leonardo Hermeling, Moritz Hitzemann, Kirsten J. Dehning and Stefan Zimmermann

Leibniz University Hannover, Institute of Electrical Engineering and Measurement Technology, Department of Sensors and Measurement Technology, Appelstr. 9A, 30167 Hannover, Germany

Contact: lippmann@geml.uni-hannover.de

Introduction

Split-ring resonators (SRRs) are structures that originate from the field of metamaterials and can induce effects such as negative permittivities and permeabilities [1]. However, there is an increasing use in various fields of sensor and measurement technology [2–4], since SRRs allow highly sensitive detection of the electromagnetic properties of a sample at or near the split capacitor. SRRs are simple electrical resonant circuits consisting of a transmission line and a ring structure with a split. Fig. 1 shows a schematic of a SRR and an equivalent simple electrical equivalent circuit.

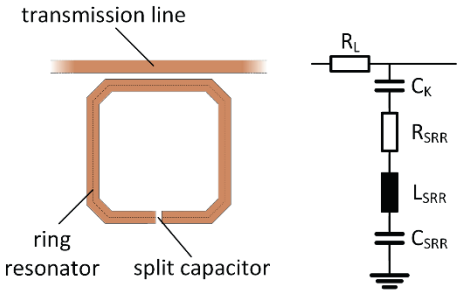

Fig 1: Schematic of a split-ring resonator (left) and a simple electrical equivalent circuit (right) with the line resistance R_L, the coupling capacitance C_K and the impedance of the ring consisting of R_SRR, L_SRR and C_SRR.

Assuming that the parasitic inductance and the capacitance to the ground of the transmission line are small compared to the capacitance to the ring, the transmission line can be approximated as an ideal ohmic resistor R_L, which is linked to the ring structure via the coupling capacitance C_K. The ring structure itself forms an RLC resonant circuit consisting of the inductance of the ring L_SRR, the ohmic resistance of the ring R_SRR, and the capacitance C_SRR. In this case, the capacitance C_SRR includes the capacitance of the split as well as the parasitic capacitances against the ground and the environment. Typically, SRRs are characterized via a transmission measurement, i.e., the amplitude ratio of received and transmitted wave. Off resonance, most of the introduced power is transferred through the transmission line, while in resonance, power transmission is significantly diminished [5]. According to the electrical equivalent circuit from Fig 1, the resonance frequency of an SRR $f_\mathrm{res,SRR}$ can be determined with the inductance L_SRR of the ring and the total capacitance $C_\mathrm{ges} = \frac{C_\mathrm{K} \cdot C_\mathrm{SRR}}{C_K + C_\mathrm{SRR}}$ as shown in Eq. 1.

$$f_\mathrm{res,SRR} = \frac{1}{2\pi \cdot \sqrt{L_\mathrm{SRR} C_\mathrm{ges}}} \qquad (1)$$

Since the inductance mainly depends on the geometric dimensions of the ring and is thus almost constant, changes in the resonance frequency of the SRR are directly related to a change in the split capacitance. The split capacitance depends on the geometric dimensions and on the permittivity of the dielectric at the split capacitor C_Split. Considering the damped SRR, changes in permittivity, but also dielectric losses, and conductivity of a sample at or near the split capacitor can be measured as a change in resonance frequency. Dielectric losses and conductivity can be also seen in the quality factor. Usually, the resonance frequency of SRRs used in sensor applications are in the triple-digit MHz range, however, the electronics must be able to accurately detect changes in the frequency in the lower Hz range [6].

Typically, the frequency response of oscillating systems, such as the SRR, is determined using a vector network analyzer. Based on the results of a sweep in excitation frequency, the resonance frequency and attenuation at resonance frequency can be determined. However, a frequency sweep with high frequency resolution to accurately determine the resonance frequency and attenuation at resonance frequency can take several seconds or even minutes. For this reason, besides costs, it is not practical to use a network analyzer for measuring rapidly changing sample properties at the split capacitance, i.e., as a detector in liquid chromatography (LC) [7,8]. In this case, the SRR may combine measurement of sample permittivity and conductivity in a single detector.

Since in LC the individual components of a liquid solution elute from the column at different times, a detector with response times of less than 1 s is required. The electronics presented in this work is designed to continuously measure the resonance frequency and attenuation at resonance frequency of a SRR within less than one second.

Concept

Continuous measurement of resonance frequency and attenuation at resonance frequency is based on the excitation of the SRR with three frequencies of equal amplitude in a single signal and individual analysis of the transmission of these three frequencies. The three frequencies consist of a center frequency and two sidebands symmetrically spaced around this center frequency. Fig. 2 shows the concept divided into signal generation, excitation of the SRR, and analysis of the received signal.

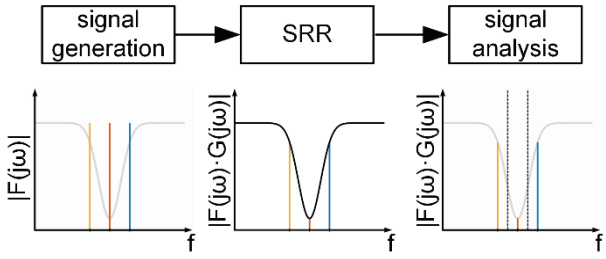

Fig 2: Concept for continuous measurement of the resonance frequency and attenuation at resonance frequency of a split-ring resonator (SRR) divided into three parts: signal generation, excitation of the SRR, and signal analysis. A signal consisting of three frequencies, a lower sideband frequency (yellow, S_{LSB}), a center frequency (red, S_{CN}), and an upper sideband frequency (blue, S_{USB}), is generated, then fed to the SRR, and the transmission of the three frequencies is analyzed individually.

By using two sidebands S_{LSB} and S_{USB} symmetrically around a center frequency, it is possible to determine the resonance frequency as well as attenuation at resonance frequency and to react to changes in resonance frequency over a wide frequency range. The amplitude response of an SRR $|G(\mathrm{j}\omega)|$ according to the equivalent circuit shown in Fig. 1 is given in Eq. 2 with the damping ratio *D*

$$D = \frac{R_{\mathrm{SRR}}}{2} \cdot \sqrt{\frac{C_{\mathrm{ges}}}{L_{\mathrm{SRR}}}},$$

the factor α

$$\alpha = \left(1 + \frac{R_{\mathrm{L}}}{R_{\mathrm{SRR}}}\right)$$

and the resonance circuit frequency ω_{res}.

$$|G(\mathrm{j}w)| = \frac{\sqrt{\omega^4 + (4D-2)\omega_{\mathrm{res}}^2\omega^2 + \omega_{\mathrm{res}}^4}}{\sqrt{\omega^4 + (4\alpha^2 D-2)\omega_{\mathrm{res}}^2\omega^2 + \omega_{\mathrm{res}}^4}} \qquad (2)$$

The amplitude response in Eq. 2 shows a symmetry in the logarithmic scale, which allows the use of the geometric mean to determine the resonance frequency. This symmetry in the logarithmic scale means that even if the center frequency is selected in a way that the amplitudes of the two sideband frequencies are equal, it differs slightly from the resonance frequency. However, in this case, the resonance frequency $f_{\mathrm{res,SRR}}$ can be calculated from the center frequency f_{CN} and the frequency spacing BW of the two sidebands according to Eq. 3.

$$f_{\mathrm{res,SRR}} = \sqrt{f_{\mathrm{CN}}^2 - \frac{BW^2}{4}} \qquad (3)$$

The attenuation at resonance frequency of the SRR can then be approximated from the attenuation of the center frequency. In particular, changes in the attenuation of a SRR can be determined with sufficient accuracy.

When the resonance frequency of an SRR changes, the center frequency can be tracked by controlling the error signal $e = |S_{\mathrm{USB}}| - |S_{\mathrm{LSB}}|$. Fig 3 shows the theoretically expected error function resulting from a sweep of the center frequency with the frequency spacing of the sidebands $BW = 10\ \mathrm{MHz}$ for a simulated SRR according to Eq. 2 with $f_{\mathrm{res,SRR}} = 500\ \mathrm{MHz}$, $D = 0{,}01$ and $\alpha = 2$.

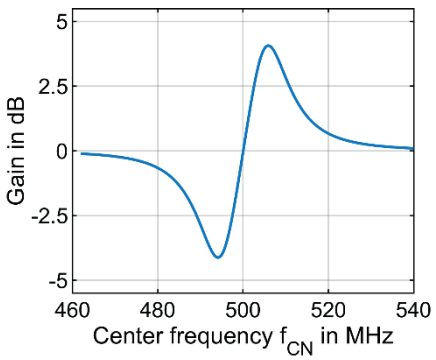

Fig 3: Simulated error function of a frequency sweep of the center frequency with a sideband frequency spacing $BW = 10\ \mathrm{MHz}$ using a simulated split-ring resonator with $f_{\mathrm{res,SRR}} = 500\ \mathrm{MHz}$, $D = 0.01$ and $\alpha = 2$.

The error function has a global minimum and a global maximum near the resonance frequency, which limits the frequency tracking to the range between the maximum and minimum. Due to the limited

linear range between the minimum and maximum, changes in resonance frequency between two successive measurements need to be smaller than the frequency spacing of the extremes from the actual resonance frequency. Besides the error function of the SRR, the maximum trackable change in resonance frequency also depends on the minimum measurement time t_{min} of the electronics, which is determined by the time for signal generation, amplitude analysis and calculation of the new center frequency for the next cycle.

Materials and Methods

The hardware implementation of the concept described above consists of a digitally controlled signal generation with analog modulation of the initial signals and analog demodulation of the received signal, as well as a digital analysis of the three frequency components. For tracking of resonance frequency over a wide frequency range, a digital controller is implemented. Alternatively, it is possible, to take a fully digital approach using a fast Digital Analog Converter (DAC) combined with a Field Programmable Gate Array (FPGA), but this approach is much more complex to implement.

The generation of the test signal, consisting of the center frequency f_{CN}, the lower sideband frequency f_{LSB} and the upper sideband frequency f_{USB} starts with the generation of three low-frequency signals and one high-frequency carrier (HF). The low-frequency sideband signal S_{BB} is generated via direct digital synthesis (DDS), with an adjustable frequency spanning 0 – 9 MHz, low-pass filtered, and post-amplified with a variable-gain amplifier. This frequency defines the frequency spacing of the two sidebands from the center frequency f_{CN} in the frequency spectrum of the test signal. In addition, an offset signal S_{offset} with a frequency of 10.7 MHz is generated, which is obtained from a 42.8 MHz crystal oscillator whose frequency is divided by a factor of four via a concatenated ring counter consisting of 2 D-flip-flops. Thus, the signal is provided in an in-phase form $S_{\mathrm{offset,I}}$ and quadrature form $S_{\mathrm{offset,Q}}$ and each of the signals is band-pass filtered and variably amplified. The offset signal allows the use of a crystal filter in the 10 MHz range for signal analysis. The HF carrier frequency S_{HF} is generated by an adjustable PLL in a frequency range from 0.1 MHz to 1.8 GHz. This signal is also low-pass filtered and provided with adjustable amplification.

The frequency spectrum of the test signal is generated from the four initial signals via several modulation steps, as shown in Fig. 4. The modulation of the signals is a modified Weaver Method, but in contrast to the original Weaver Method, the frequency components of the low-frequency offset signal are not suppressed, since these are required to generate the center frequency. The two amplitude modulations (AM) of S_{BB} with $S_{\mathrm{offset,I}}$ and S_{BB} with $S_{\mathrm{offset,Q}}$ generate the two low-frequency intermediate signals $S_{\mathrm{NF,I}}$ and its Hilbert transform $S_{\mathrm{NF,Q}}$. These intermediate signals are fed to the baseband inputs of an IQ modulator and shifted into the high-frequency range by mixing with the HF carrier signal S_{HF}. This modulation generates the test signal S_{test} with a center frequency $f_{\mathrm{CN}} = f_{\mathrm{HF}} + f_{\mathrm{offset}}$ and the two sidebands $f_{\mathrm{LSB}} = f_{\mathrm{CN}} - \frac{f_{\mathrm{BB}}}{2}$ and $f_{\mathrm{USB}} = f_{\mathrm{CN}} + \frac{f_{\mathrm{BB}}}{2}$.

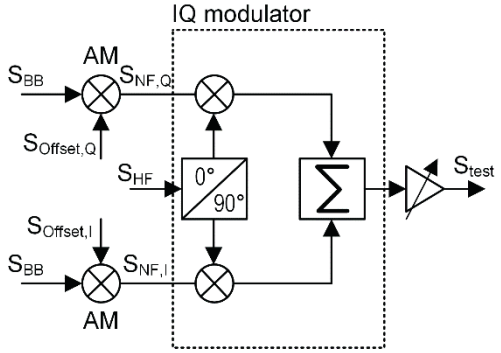

Fig 4: Block diagram for generating the test signal for excitation of a SRR. The test signal S_{test} is generated by two amplitude modulations (AM) of the low-frequency sideband signal S_{BB} with the in-phase offset signal $S_{offset,I}$ and the quadrature offset signal $S_{offset,Q}$ followed by IQ modulation of the intermediate signals $S_{NF,I}$ and $S_{NF,Q}$ with the HF carrier signal S_{HF}.

Fig. 5 shows the block diagram of the demodulator circuit used for the analysis of the received signal. In a first step, the received signal from the SRR S_{SRR} is mixed down with the HF signal S_{HF} and a band-pass filter at the output of the mixer suppresses the upper sideband generated during mixing. This approach allows the use of narrow-band crystal filters in the 10 MHz range independent of the resonance frequency of the SRR. The signal is then processed in parallel branches. A notch filter separates the sidebands from the center frequency, while in the other branch a band-pass filter extracts the center frequency. The intensity of the center signal is then analyzed directly with a detector (DET). In the parallel branch, the lower sideband is analyzed after another low-pass filter following the band-stop filter, while for the upper sideband, the spectrum has to be inverted and then low-pass filtered to separate it from the lower sideband before it can be analyzed.

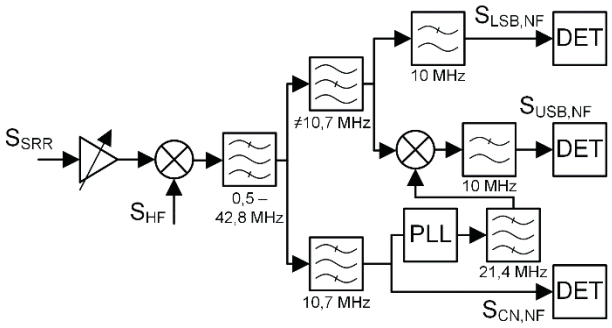

Fig 5: Block diagram of the demodulation of the received signal S_{SRR}. First, the signal is mixed down with the HF carrier S_{HF} and band-pass filtered. The sidebands and the center frequency are analyzed in parallel branches after a band-pass and a band-stop filter. The center frequency $S_{\mathrm{CN,NF}}$ is then directly analyzed with a detector (DET). The lower sideband $S_{\mathrm{LSB,NF}}$ is low-pass filtered before being fed to a detector. The spectrum of the upper sideband $S_{\mathrm{USB,NF}}$ is inverted and low-pass filtered before being fed to a detector.

Signal generation, acquisition of the amplitudes of the received signal and tracking of the resonance frequency is controlled by an external microcontroller, which is connected via USB to a computer. The printed circuit board developed in this work is shown in Fig. 6.

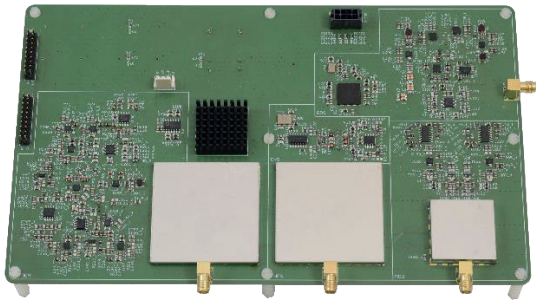

Fig 6: Photo of the electronics for the continuous measurement of the resonance frequency and attenuation of a SRR.

In all measurements, the electronics was tested in combination with an SRR consisting of a transmission line on PCB (FR4) and a stainless-steel capillary split-ring structure forming the split-ring resonator (CaSRR) as used in Hitzemann et al. [6]. This CaSRR is specifically developed for liquid analysis in LC applications.

In a first measurement, the amplitude response of the CaSRR was determined when rinsed with pure water and acetonitrile with a sweep of the center frequency. For comparison, the same measurement was subsequently performed using a commercial vector network analyzer (Rhode and Schwarz, ZNL6).

To investigate the tracking on changes in resonance frequency of the CaSRR, a sweep of the center frequency was recorded while the CaSRR was rinsed with pure water. The error signal was determined from the attenuation of the upper and lower sideband frequency. Finally, a solvent gradient of ultrapure water and acetonitrile generated with a Knauer high performance LC (HPLC) system was recorded. The HPLC consists of a solvent reservoir, a binary high-pressure pump P 6.1L with two 10 mL-heads, a degasser and a high-pressure mixing chamber, a 6-port-injection valve with 20 µL sample loop, a HPLC-column in a column thermostat CT 2.1. The program started with pure water for 2 min, followed by a linear ramp of acetonitrile concentration from 0% to 100% during 2 min, hold for 2 min, and a linear ramp down from 100% to 0% acetonitrile during 2 min.

The chemicals acetonitrile (Sigma product: 1037252002) and ultrapure water (Sigma product: 1037282002) were purchased from Sigma-Aldrich, Germany, with a purity of > 99%.

Results and Discussion

Fig. 7 shows the results of comparative measurements of the resonance frequency of the CaSRR rinsed with pure water (top) and rinsed with acetonitrile (bottom). The data of the commercial network analyzer are shown in blue, and those from the electronics developed here are shown in orange. For the measurement with pure water, the difference in the measured resonance frequency is 2.976 MHz, and for the measurement of acetonitrile, the difference is 0.389 MHz. The difference in the measured attenuation at resonance frequency between the commercial ZNL6 and our electronics is 0.224 dB for pure water, while there is a larger difference of 4.06 dB for acetonitrile. A possible explanation for the discrepancies between these two detectors could be an insufficient suppression of the image frequency, which leads to additive interference in superheterodyne receivers such as those used for the demodulation.

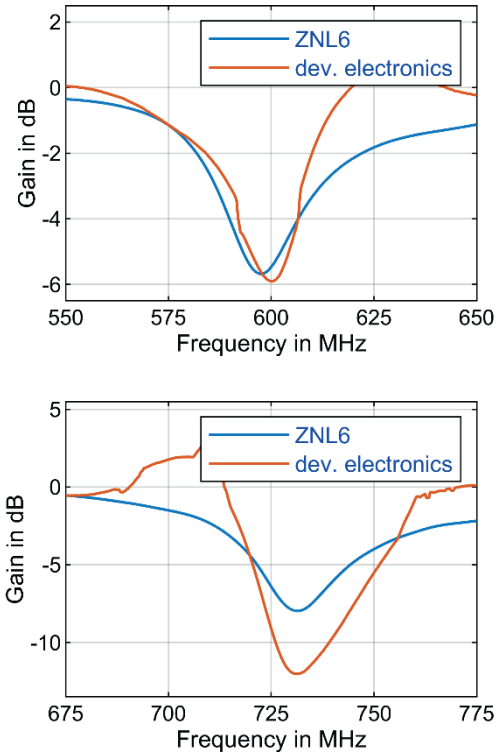

Fig 7: Comparison of the measured values obtained with the electronics shown in Fig 6 (orange) and a ZNL6 from Rohde and Schwarz (blue) for the capillary split-ring resonator rinsed with pure water (top) and with acetonitrile (bottom).

The error signal of the CaSRR rinsed with pure water is shown in Fig 8. Comparing this with the shape of the theoretically expected curve, as shown in Fig. 3, it can be seen that the error signal is not symmetrical around the resonance frequency. This is mainly due to the asymmetry of the frequency response of the CaSRR causing the asymmetry of the error signal. Nevertheless, the error signal has a linear range near the resonance frequency, allowing for tracking the resonance frequency with reasonable accuracy of 150 kHz.

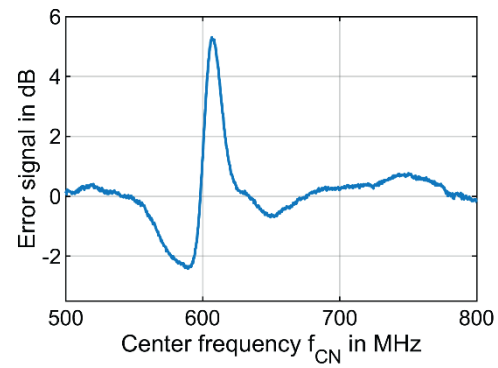

Fig 8: Error signal of the capillary split-ring resonator rinsed with pure water, measured with the electronics presented in Fig 6.

Finally, tracking of the resonance frequency of the CaSRR was tested with a solvent gradient of water and acetonitrile. The results shown in Fig. 9 clearly demonstrate that the control circuit allows the test signal to track the changes in resonance frequency over the entire range of about 130 MHz, thus responding to the change in electromagnetic properties of the liquid. These results confirm that the considerations on tracking the resonance frequency developed in theory could also be implemented in practice with the electronics presented in this work.

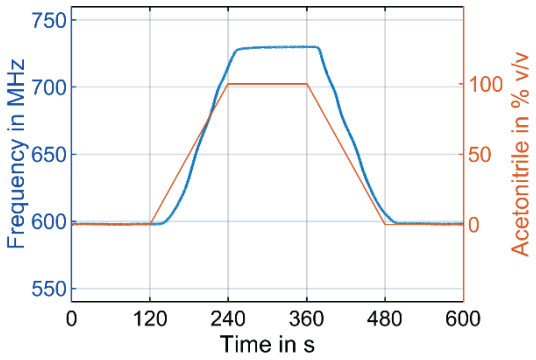

Fig 9: Measurement of a solvent gradient of water and acetonitrile with the electronics shown in Fig 6. The solvent gradient is shown in orange, and the resonance frequency is shown in blue.

Conclusion

In this paper, we present a new concept and the hardware implementation in electronics for continuous measurement of resonance frequency and attenuation at resonance frequency of SRRs. First measurements demonstrate feasibility. In particular, it is shown that the resonance frequency of a SRR can be tracked over a wide frequency range, which allows the use of SRRs as a detector in LC or HPLC. In future work, the remaining deviations between the measurements with our new electronics and a commercial network analyzer will be further investigated. Additionally, the mentioned CaSRR will be tested together with our new electronics as a HPLC detector.

References

[1] Smith, Padilla, Vier, Nemat-Nasser, Schultz, Composite medium with simultaneously negative permeability and permittivity, Physical Review Letters 84, 4184–4187 (2000); doi: 10.1103/PhysRevLett.84.4184.

[2] D. J. Rowe, S. al-Malki, A. A. Abduljabar, A. Porch, D. A. Barrow, C. J. Allender, Improved Split-Ring Resonator for Microfluidic Sensing, IEEE Transactions on Microwave Theory and Techniques 62, 689–699 (2014); doi: 10.1109/TMTT.2014.2299514.

[3] T. Chretiennot, D. Dubuc, K. Grenier, A Microwave and Microfluidic Planar Resonator for Efficient and Accurate Complex Permittivity Characterization of Aqueous Solutions, IEEE Transactions on Microwave Theory and Techniques 61, 972–978 (2013); doi: 10.1109/TMTT.2012.2231877.

[4] M. Schueler, C. Mandel, M. Puentes, R. Jakoby, Metamaterial Inspired Microwave Sensors, IEEE Microwave Magazine 13, 57–68 (2012); doi: 10.1109/MMM.2011.2181448.

[5] T. Reinecke, J.-G. Walter, T. Kobelt, A. Ahrens, T. Scheper, S. Zimmermann, Design and evaluation of split-ring resonators for aptamer-based biosensors, Journal of Sensors and Sensor Systems 7, 101–111 (2018); doi: 10.5194/jsss-7-101-2018.

[6] M. Hitzemann, K. J. Dehning, A. V. Gehl, E.-F. Sterr, S. Zimmermann, Fast Readout of Split-Ring Resonators Made Simple and Low-Cost for Application in HPLC, Electronics 11, 1139 (2022); doi: 10.3390/electronics11071139.

[7] A. Gehl, S. Zimmermann, Ein neues Detektorkonzept für die Flüssigchromatographie basierend auf einem Split-Ring-Resonator / A new detector concept for liquid chromatography based on a split-ring resonator, tm - Technisches Messen 85, s33-s37 (2018); doi: 10.1515/teme-2018-0032.

[8] K. J. Dehning, M. Hitzemann, E.-F. Sterr, S. Zimmermann, P8.9 - Split-Ring Resonator as Detector for Liquid Chromatography, Dresdner Sensor-Symposium, 285–289 (2021); doi: 10.5162/15dss2021/P8.9.